

# Fast Visibility Restoration from a Single Color or Gray Level Image

Jean-Philippe Tarel      Nicolas Hautière  
LCPC-INRETS (LEPSIS),  
58 Boulevard Lefèvre, F-75015 Paris, France  
tarel@lcpc.fr      hautiere@lcpc.fr

## Abstract

*One source of difficulties when processing outdoor images is the presence of haze, fog or smoke which fades the colors and reduces the contrast of the observed objects. We introduce a novel algorithm and variants for visibility restoration from a single image. The main advantage of the proposed algorithm compared with other is its speed: its complexity is a linear function of the number of image pixels only. This speed allows visibility restoration to be applied for the first time within real-time processing applications such as sign, lane-marking and obstacle detection from an in-vehicle camera. Another advantage is the possibility to handle both color images or gray level images since the ambiguity between the presence of fog and the objects with low color saturation is solved by assuming only small objects can have colors with low saturation. The algorithm is controlled only by a few parameters and consists in: atmospheric veil inference, image restoration and smoothing, tone mapping. A comparative study and quantitative evaluation is proposed with a few other state of the art algorithms which demonstrates that similar or better quality results are obtained. Finally, an application is presented to lane-marking extraction in gray level images, illustrating the interest of the approach.*

## 1. Introduction

In surveillance, intelligent vehicles, and remote sensing systems, the image appearance is subject to weather conditions and thus affected by haze, fog and smoke. On a gray level image, the model of the effect of the fog is established by Koschmieder as the following relationship [4]:

$$L(x, y) = L_0(x, y)e^{-kd(x, y)} + L_s(1 - e^{-kd(x, y)}) \quad (1)$$

where  $L(x, y)$  is the apparent luminance at pixel  $(x, y)$ ,  $d(x, y)$  is the distance of the corresponding object with intrinsic luminance  $L_0(x, y)$ ,  $L_s$  is the luminance of the sky and  $k$  denotes the extinction coefficient of the atmosphere.

This model is directly extended to a color image by applying the same model on each RGB component, assuming a camera with a linear response. The first effect of the fog is an exponential decay  $e^{-kd(x, y)}$  of the intrinsic luminance  $L_0(x, y)$  and of the intrinsic colors. Thus, the contrast of the object is reduced and thus its visibility in the scene. The second effect is the addition of a white atmospheric veil  $L_s(1 - e^{-kd(x, y)})$  which is an increasing function of the object distance  $d(x, y)$ .

The presence of fog in an image is generally a source of difficulties when processing by an algorithm designed for clear weather images. Instead of extending each of algorithm from clear to foggy weather, it seems more adequate to perform on each input image a visibility restoration pre-processing. This pre-processing can be applied only when fog is detected, see for example [4], to save even more computational time. Visibility restoration is an ill-posed problem. Indeed, the atmospheric veil being a function of the objects depth, a perfect visibility restoration requests the estimation of the true colors of the objects ( $L_0(x, y)$ ) and of the fog properties ( $k$  and  $L_s$ ) as well as the depth-map  $d(x, y)$  of the scene.

As a consequence, approaches based on the use of several images of the scene were proposed: using images at different times [8] or using images with different polarizing filters [11]. This kind of methods are very constraining for the acquisition and cannot be used on existing image databases. An alternative of using several images is to use an approximate depth-map of the image scene, or the exact depth-map when available, as proposed in [7, 2, 6]. These methods are more flexible but they are application dependent or require interactions with an expert. For more detailed review on visibility restoration algorithms in the computer vision and computer graphics fields, the reader is referred to [1, 6].

Very recently and for the first time in [1, 12, 5], three approaches were proposed which work from a single image without using any other extra source of information. In [1], the proposed algorithm is deeply based on the color and thus cannot deal with a gray level image. The algorithm is computationally intensive. In comparison, the algorithm in [12]

does not always achieve equally good results on very saturated scenes, but it has the great advantage of being more generic and thus of easier application on many kinds of images. In particular, it works on color images as well as on gray level images. The algorithm in [5] also works on gray-level and color images. However, the disadvantage of these last two algorithms is a processing time of 5 to 7 minutes and of 10 to 20 seconds on a  $600 \times 400$  image, respectively.

We here propose a novel algorithm for visibility restoration based on a filtering approach. It is much faster compared to [1, 12, 5] since its complexity is only a linear function of the number of input image pixels, and it is able to achieve equally and sometime even better results to both color and gray level images. In section 2, our approach and the steps of the fast visibility restoration algorithm are detailed and a variant with a smoothing algorithm preserving edges and corners with obtuse angles is introduced. In section 3 is provided a comparison with algorithms [1, 12, 6, 5] based on a quantitative evaluation on four color images, illustrating the pros and cons of the proposed algorithm. Finally, in section 4, the interest of the visibility restoration for intelligent vehicles and in particular lane-marking detection is detailed.

## 2. Visibility Restoration Algorithm

When no depth information is available, as noticed in [12], it is not possible in Koschmieder's law (1) to separate between the contribution of the extinction coefficient of the atmosphere  $k$  and the scene distance map  $d$ . As a consequence, introducing the intensity of the atmospheric veil  $V(x, y) = I_s(1 - e^{-kd(x, y)})$ , Koschmieder's law can be rewritten in gray level and in colors as:

$$I(x, y) = R(x, y)\left(1 - \frac{V(x, y)}{I_s}\right) + V(x, y) \quad (2)$$

where  $I(x, y)$  is the observed image intensity (gray level or RGB) at pixel  $(x, y)$  and  $R(x, y)$  is the image intensity without fog. As a consequence, from now on, instead of seeking to infer the depth-map  $d(x, y)$ , we will infer equivalently the atmospheric veil  $V(x, y)$ . The visibility restoration algorithm can thus be decomposed into several steps: estimation of  $I_s$ , inference of  $V(x, y)$  from  $I(x, y)$ , estimation of  $R(x, y)$  by inverting (2), smoothing to handle noise amplification and final tone mapping.

### 2.1. White Balance

We assume that the white balance is performed prior to the visibility restoration algorithm. When the white balance is correctly performed, the fog being pure white, this implies that  $I_s$  can be set to  $(1, 1, 1)$ , also assuming that the input image  $I(x, y)$  is normalized between 0 and 1. Thanks to the presence of fog in the image, most of time the white

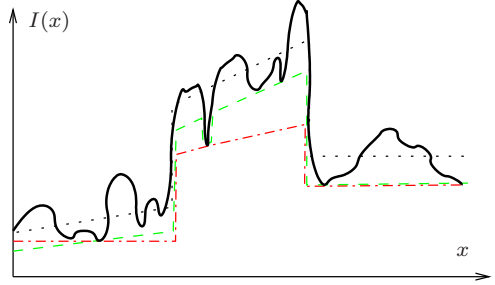


Figure 1. The amount of white color  $W$  is the black continuous curve and its local average is the black dash line. The result  $V$  estimated by optimizing (3) for a large value of  $\lambda$  is shown as red dot-dash. The result  $V$  obtained with the proposed approach is shown as green dash.

balance can be performed simply by biasing the image average color towards pure white. For difficult images where light color changes along the image, such as in Fig. 8, it is better to perform a local white balance by biasing towards local image averages.

### 2.2. Atmospheric Veil Inference

The first step of image restoration consists in inferring the atmospheric veil  $V(x, y)$ . Due to its physical properties, the atmospheric veil is subject to two constraints when the observed image is known: it is positive  $0 \leq V(x, y)$  and being pure white, for each pixel, it can not be higher than the min of the components of  $I(x, y)$ . We thus compute the image  $W(x, y) = \min(I(x, y))$  defined as the image of the minimal component of  $I(x, y)$  for each pixel (gray level or RGB).  $W$  is the image of the whiteness within the observed image  $I$ . For a gray level image, we obviously have  $W = I$ . The second constraint can thus be written as  $V(x, y) \leq W(x, y)$ .

Following [12], visibility restoration is an ill-posed problem and a regularized solution can be obtained by maximizing the contrast of the resulting image assuming that the depth-map must be smooth except along edges with large depth jumps. The problem can thus be reformulated as maximizing  $V(x, y)$  assuming that  $V(x, y)$  is smooth most of the time, and formalized as the following optimization problem:

$$\operatorname{argmax}_V \int_{(x,y)} V(x, y) - \lambda \phi(\|\nabla V(x, y)\|^2) \quad (3)$$

with constraints  $0 \leq V(x, y) \leq W(x, y)$ . Parameter  $\lambda$  controls the smoothness of the solution,  $\phi$  is an increasing concave function allowing large jumps.

The optimization of (3) being too computationally intensive, we search for another way to deal with the visibility restoration problem allowing real time processing. A possibility consists in performing a spatial erosion. Notice that



Figure 2. From left to right, the original image, the atmospheric veil  $V(x, y)$  and the restoration obtained by enforcing complete smoothness, the atmospheric veil  $V(x, y)$  and the restoration obtained by enforcing smoothness most of the time (used parameters in both cases  $p = 0.95$ ,  $s_v = 41$  and  $s_i = 19$ ).



Figure 3. From left to right, the original image, the image and a zoom after restoration using the median filter, the image and a zoom using the filter we named median of median along lines (used parameters in both cases  $p = 0.95$ ,  $s_v = 61$  and  $s_i = 1$ ).

the first step of [5] is close to an erosion on  $W$  since it consists in an erosion on each color component followed by a min over the components. We also experiment with the erosion and we found that it suffers of halo. This is why a refinement using matting is requested in [5]. The problem can be seen as a filtering problem. We thus search for other operators that can be used with advantages in particular to improve robustness of the result.

The optimization of (3) consists in searching for a function  $V(x, y)$  of maximum volume, smooth most of the time and lower than  $W(x, y)$ . In Fig. 1, the obtained  $V(x)$  is shown as a red dot-dash curve for a large value of  $\lambda$ , the black continuous curve being  $W(x)$ . Due to the constraint  $V(x) \leq W(x)$ , the deep valley of  $W(x)$  in the middle of the figure forces  $V(x)$  to relatively small values around this position. These small values may be justified when the middle of the scene is at a similar distance. In such a case, the presence of this valley indicates that the scene contains objects with colors weakly saturated. On the contrary, this valley may be due to a dark small and closer object such as a bird. In such a case, this valley should be considered as outliers in estimating locally  $V$ , and thus a curve such as the green one in Fig. 1 must be preferred, to avoid keeping a certain amount of fog around outliers. To tackle this robustness problem, we propose to infer  $V(x, y)$  as a percentage of the difference between the local average of  $W(x, y)$  and the local standard deviation of  $W(x, y)$ .

It is now important to stress that the introduction of possible large jumps is necessary to restore images such as the one in Fig. 2. This figure shows the resulting difference when enforcing complete smoothness or smoothness most of the time of the atmospheric veil. Indeed, if the obtained atmospheric veil  $V(x, y)$  does not seem so dif-

ferent, an incorrect halo appears when complete smoothness is enforced. This implies that the local average of  $W(x, y)$  must be performed using a smoothing algorithm which preserves large jumps along edges. Fig. 1 shows in black dot line the resulting local average. To perform an edge preserving smoothing, robust bilateral filters can be used or faster the median filter which is a particular bilateral filter. The local average of  $W$  is thus computed as  $A(x, y) = \text{median}_{s_v}(W)(x, y)$  where  $s_v$  is the size of the square or disc window used in the median filter. Then to take into account that areas with contrasted texture are probably not foggy, the local standard deviation of  $W(x, y)$  is subtracted to  $A(x, y)$ . Again, to be robust to outliers, this standard deviation must be estimated in a robust way, for instance by applying the median filter on  $|W(x, y) - A(x, y)|$ . The third and last step consists in multiplying  $B(x, y) = A - \text{median}_{s_v}(|W - A|)$  by factor  $p$  in  $]0, 1[$  to control the strength of the visibility restoration. The values of  $pB(x, y)$  do not necessarily respect the constraints on  $V$  and thus are thresholded (to obtain the final green dash curve of Fig. 1). In summary, the atmospheric veil  $V$  is inferred as:

$$\begin{aligned} V(x, y) &= \max(\min(pB(x, y), W(x, y)), 0) \\ \text{with } B(x, y) &= A(x, y) - \text{median}_{s_v}(|W - A|)(x, y) \\ \text{and } A(x, y) &= \text{median}_{s_v}(W)(x, y) \end{aligned} \quad (4)$$

Fig. 2 shows an example of inferred atmospheric veil using (4) with  $p = 0.95$  and  $s_v = 41$ .

### 2.3. Corner Preserving Smoothing

To compute  $A$ , we previously used the classical median filter which preserves edges but not corners. This may induce artifacts for large values of  $s_v$  on very structured



Figure 4. From left to right, the original image, the results obtained with  $p = 0.7$  and  $s_v = 61$ ,  $p = 0.90$  and  $s_v = 61$ ,  $p = 0.98$  and  $s_v = 61$ ,  $p = 0.90$  and  $s_v = 21$  ( $s_i = 1$ ). Notice how the restoration is too strong with  $p = 0.98$  and too light with  $p = 0.7$ . It seems better with  $p = 0.9$ . On the right, white markings close to the vehicle are erased due to a too small value of  $s_v = 21$  compared to the lane-marking size.  $s_v = 61$  leads to better results.



Figure 5. From left to right, the original image, the image and a zoom after restoration without and with smoothing adapted to contrast magnification ( $s_v = 61$ ,  $p = 0.95$  and  $s_i = 19$ ). Notice how jpeg artifacts are softened.

scenes such as cities, buildings. We thus now introduce an original filter we named *Median of Median Along Lines* which is able to preserve edges as well as corners with obtuse angle. Assuming an a priori set of  $n_v$  centered line segments  $S_i$ ,  $1 \leq i \leq n_v$  of uniformly sampled orientations is given, this filter consists in the same local processing at each pixel. Each segment is of length  $s_v$ . For each pixel and for each segment  $S_i$  centered on the current pixel, the median value of the intensities along  $S_i$  is computed and saved as  $m_i$ . When the  $m_i$  are collected for the current pixel and whole centered segments, the filtered image pixel is computed as the median value of the  $m_i$  with  $1 \leq i \leq n_v$ .

When the current pixel is close to an edge, all  $m_i$  are close to the average intensity  $I$  of the region where the current pixel is. As a consequence, the proposed filter preserves edges. When the current pixel is close to a corner with angle  $\theta$ , the percentage of values  $m_i$  not close to  $I$  equals  $1 - \frac{|\theta|}{\pi}$ . As a consequence, for obtuse angle only, this percentage is higher than 50% and thus the median of the  $m_i$  is close to  $I$ . This implies that the median of median along lines filter preserves edges as well as corners with an obtuse angle. Due to this last property, median of median along lines filter can be used with advantages in many other image processing applications.

Fig. 3 shows the interest of using the median of median along lines filter ( $n_v = 5$ ) compared to the classical median filter on a image, see in particular around the tree trunk. With this last filter, the proposed restoration algorithm is not real-time, but can be still quite fast when using a reduced set of segments  $S_i$ .

## 2.4. Image Visibility Restoration

Now that the atmospheric veil  $V$  has been inferred, the restoration of the original image colors can be performed by solving (2) with respect to  $R$ :

$$R(x, y) = \frac{I(x, y) - V(x, y)}{1 - \frac{V(x, y)}{I_s}} \quad (5)$$

In (4), the two parameters  $p$  and  $s_v$  are used to control the aspect of the visibility restoration. The value of  $p$  controls the strength of the restoration, and is set usually between 90 and 95%. This means that 90% or 95% of the amount of atmospheric veil is removed. This parameter is useful to compromise between a) highly restored visibility (when  $p$  is closed to 1) where colors may appear over saturated and too dark, and b) less restored visibility where colors are less saturated and thus clearer, as illustrated in Fig. 4 on a gray level image. The parameter  $s_v$  specifies the larger size of the assumed white objects. Any close to white object with a size larger than  $s_v$  is assumed to be white because of the fog. On the contrary, a white object with a size smaller than  $s_v$  will be assumed intrinsically as white. This is illustrated in Fig. 4 with white lane-markings in the bottom of the image.

## 2.5. Smoothing Adapted to Contrast Magnification

During the image visibility restoration, the more the atmospheric veil is important, the more the contrast is increased. This also leads to increasing noise and image compression artifacts. As shown in Fig. 5, the original image is compressed using jpeg, and after the visibility restoration, the compression artifacts become clearly visible. To



Figure 6. From left to right, the original images, the results obtained by [1], our results with  $p = 0.95$ ,  $s_v = 41$  and  $s_i = 1$ .

soften the noise and artifacts, an local smoothing is thus required. This local smoothing must be adapted to the contrast magnification factor  $\gamma = \frac{1}{1 - \frac{V(x,y)}{I_s}}$  within (5). A noise of standard deviation  $\sigma$  becomes a noise of std  $\gamma\sigma$  after image restoration. By averaging on a window of size  $s \times s$ , the std becomes  $\frac{1}{\sqrt{s^2}}\gamma\sigma$ . As a consequence, to come back to a noise of std  $\sigma$ ,  $s$  must be equal to the contrast factor  $\gamma$ . We thus choose for the locally adapted smoothing to perform a median filter with a square window of size  $s \times s$  where  $s$  equals the integer part of the contrast factor  $\gamma$ . This rule to set  $s$  may lead to an over-sized window in very foggy areas. Therefore, we added an extra parameter  $s_i$  which sets the maximum size of the adapted window. In Fig. 5, the restoration result where the jpeg artifacts are softened due to the adapted smoothing is shown ( $s_i = 19$ ). When  $s_i = 1$ , this indicates that the effect of the adapted smoothing is canceled.

## 2.6. Dedicated Tone Mapping

Previously, we described the different steps of the visibility restoration considering that the image is in float format. The obtained restored images are usually with a higher dynamic than the original one. Therefore, the last step rarely described in visibility restoration but important for visualization consists in the tone mapping. The same tone mapping procedure is important to allow the visual comparison of the resulting images obtained by different visibility restoration algorithms and also for comparison with the original image. To have a resulting image with not too far different aspects compared to the original image, we ap-

ply a linear mapping on the log original and log resulting images which enforces that the corresponding images have similar mean and std in the bottom third part of the image. The bottom third is used since it usually corresponds to the part of the image with less fog. Denote  $a_I$  and  $d_I$  the mean and std of the log original image  $\log(I(x,y))$  in the bottom third part, and  $a_R$  and  $d_R$  the mean and std of the log restored image  $\log(R(x,y))$  also in the bottom third part. The first step of the tone mapping consists in computing  $U(x,y) = R(x,y)^{\frac{d_L}{d_R}} e^{a_I - a_R \frac{d_L}{d_R}}$ .

Then the high intensity dynamic of the resulting image is compressed using a function inspired by [10]. The final tone mapped image  $T(x,y)$  is obtained by non-linear mapping  $T(x,y) = \frac{U(x,y)}{1 + (\frac{1}{255} - \frac{1}{M_G})G(x,y)}$ , where  $G(x,y)$  are the gray levels of  $U(x,y)$  and  $M_G$  is the maximum of  $G$ . The obtained image  $T$  is always in  $[0, 255]$ .

## 3. Comparison Experiments

The visibility restoration algorithm is controlled by three parameters:  $p$  which is the percentage of removed atmospheric veil,  $s_v$  the assumed maximum size of white objects in the image (see Fig. 4),  $s_i$  the maximum size of the adapted smoothing to soften the noise amplified by the restoration (see Fig. 5).

### 3.1. Complexity

For an image of size  $s_x \times s_y$ , the complexity of the proposed visibility restoration algorithm is  $O(s_x s_y s_v^2 \ln s_v)$  when using brute-force implementation of the median fil-



Figure 7. From left to right, the original image, the result obtained by [1], our result with  $p = 0.95$ ,  $s_v = 11$  and  $s_i = 1$ .

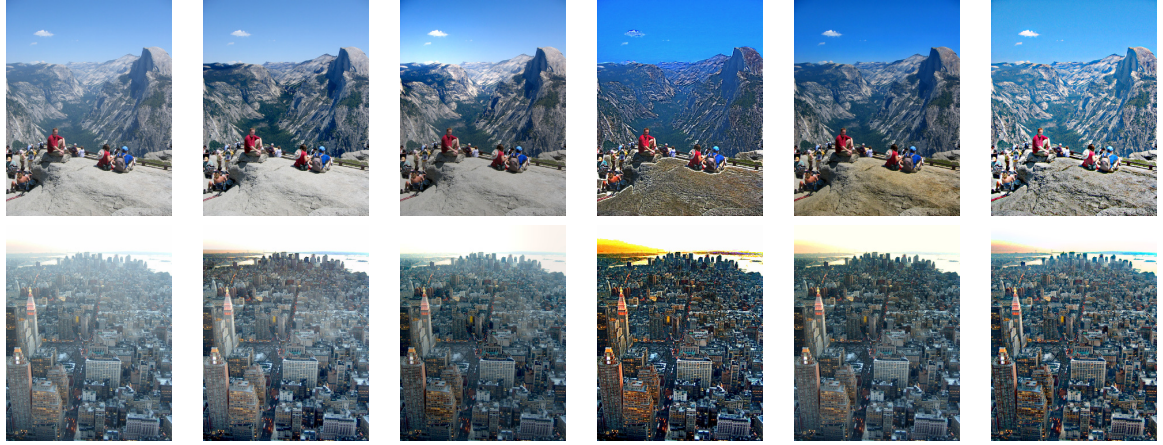


Figure 8. From left to right, the original image and the results obtained by Kopf&al. [6], Fattal [1], Tan [12], He&al. [5] and our algorithms. See more results in <http://perso.lcpc.fr/tarel.jean-philippe/visibility>.

ter, the adapted smoothing being neglected. By using the median of median along lines filter, complexity is  $O(s_x s_y n_v s_v \ln s_v)$ . In [9], a fast implementation of the median filter in  $O(s_x s_y)$  is proposed. Thanks to this fast median filter, the complexity of the proposed visibility restoration algorithm is also  $O(s_x s_y)$ , i.e., it is a linear function of the number of input image pixels whatever the value of  $s_v$ . For instance, 0.17 second is needed to obtain the second image in Fig. 5 which is of size  $759 \times 574$  ( $s_v = 61$  and  $s_i = 1$ ).

### 3.2. Qualitative Comparison

Fig. 6 shows a comparison between results obtained by [1] and our algorithm. In the first column are the original images, and in the second the results obtained by [1]. The last column displays the obtained results with  $p = 0.95$ ,  $s_v = 41$  and  $s_i = 1$ . The first line illustrates an inconvenience of our algorithm compared to [1]: it is not able to remove the fog between the small leaves. This is due to the fact that we used a geometric criterion to decide if the observed white is due to the fog or to the color of the observed object. On the contrary, the criterion used in [1] is based on color, and thus the algorithm can not be applied to a gray level image. An advantage of our algorithm is its ability to

better remove the fog in the bottom of the first image and at long distance in the second image.

Fig. 7 shows an example of image in presence of inhomogeneous fog. The first and second image display the original image and the result obtained by [1]. Notice how the second image is uniformly green compared to our result. To process this image and remove locally inhomogeneous fog, the smoothing scale on atmospheric veil must be set to the rather small value  $s_v = 11$ . The original image being of good quality, no image smoothing is performed ( $s_i = 1$ ).

Fig. 8 allows the comparison of our results with four state of the art visibility restoration algorithms: Kopf&al. [6] which uses 3D information on the scene, Fattal [1] which is based on a chroma criterion, Tan [12] and He&al. [5] which are based on a geometric criterion. Notice that the results obtained with our algorithm seems visually close to the results obtained by Kopf&al. and He&al., with less saturated colors compared with Tan, thanks to the local white balance preprocessing.

### 3.3. Quantitative Evaluation

To quantitatively assess and rate these four methods, we use the method dedicated for visibility restoration proposed in [3]. This method computes three indicators  $e$ ,  $\bar{r}$  and  $\Sigma$

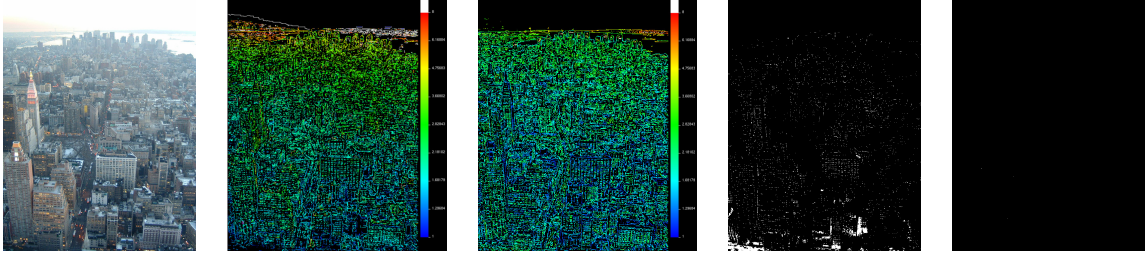


Figure 9. From left to right, the original image, the map of ratio  $r$  of the gradients at visible edges for Tan [12] and for our algorithm, the map of pixels becoming completely black or completely white for Tan and for our algorithm. The corresponding restored images are the last two images of Fig. 8.

Table 1. Rate  $e$  of new visible edges produced by the five compared methods on four images.

$e$	Kopf&al.	Fattal	Tan	He&al.	Our
ny12	0.05	-0.06	-0.14	0.06	0.07
ny17	0.01	-0.12	-0.06	0.01	-0.01
y01	0.09	0.04	0.08	0.08	0.024
y16	-0.01	0.03	-0.08	0.06	-0.008

Table 2. Mean ratio  $\bar{r}$  of the gradients at visible edges obtained by the five compared methods on four images.

$\bar{r}$	Kopf&al.	Fattal	Tan	He&al.	Our
ny12	1.42	1.32	2.34	1.42	1.88
ny17	1.62	1.56	2.22	1.65	1.87
y01	1.62	1.23	2.28	1.33	2.09
y16	1.34	1.27	2.08	1.42	2.01

Table 3. Percentage of pixels which becomes completely black or completely white after restoration for the five compared methods on four images.

$\Sigma$	Kopf&al.	Fattal	Tan	He&al.	Our
ny12	0.002	0.086	0.02	0.0	0.0
ny17	0.013	0.020	0.008	0.001	0.0
y01	0.0002	0.015	0.005	0.007	0.0
y16	0.003	0.003	0.005	0.002	0.0

allowing to compare two gray level images: the input image and the restored image. The visible edges in the image before and after restoration are selected by a 5% contrast thresholding. This allows to compute the rate  $e$  of edges newly visible after restoration. Then, the mean  $\bar{r}$  over these edges of the ratio of the gradient norms after and before restoration is computed. This indicator  $\bar{r}$  estimates the average visibility enhancement obtained by the restoration algorithm. At last, the percentage of pixels  $\Sigma$  which becomes completely black or completely white after restoration is

computed.

These indicators  $e$ ,  $\bar{r}$  and  $\Sigma$  are evaluated for Kopf&al. [6], Fattal [1], Tan [12], He&al. [5] and our algorithms on four images, see Tab. 1, Tab. 2 and Tab. 3. Used parameters are  $s_v = 41$ ,  $s_i = 1$ ,  $p = 0.9$  with local white balance. Results on images y16 and ny12 can be seen on Fig. 8. From Tab. 1, we deduce that depending of the image, Kopf&al., Fattal, Tan and our algorithms may remove visible edges, contrary to He&al. algorithm. From Tab. 2, we can order the five algorithms in decreasing order with respect to average increase of contrast on visible edges: Tan, our, He&al., Kopf&al. and Fattal. This confirms our observations on Fig. 6, Fig. 7 and Fig. 8. The results in Tab. 2 must be balanced. Indeed, if visibility restoration algorithms must increase the contrast, artificial edges must not becomes visible. In Fig. 9 is shown the maps of the ratio  $r$  of the gradients at visible edges for Tan and our algorithm, and one can notice than extra edges appear in the sky with Tan's algorithm. This indicates that the contrast has been increased probably too strongly. Tab. 3 gives the percentage of pixels which become completely black or completely white after the restoration. Compared to others, our and He&al. algorithms give the smallest percentages. These perturbed pixels are shown in white in Fig. 8 for Tan and our algorithm.

## 4. Application

The evaluation of visibility restoration is difficult on real images since no reference is available. To demonstrate the interest of the proposed visibility restoration algorithm in the context of intelligent vehicles, after lane-marking extraction, we evaluate the obtained results with and without restoration on a database of 12 images with ground-truth. The 12 images were extracted from two different sequences with fog. Each of these images was manually labeled with lane-marking and non-lane-marking labels. We use the classical evaluation by the Receiver Operating Characteristic (ROC) curve completed with the Dice curve, following [13]. Two extraction algorithms are tested: the simple

Global Threshold (GT) and the Symmetric Local Threshold (SLT) which gives best results in comparison [13]. The ROC curves in Fig. 10 shows the large gain obtained when using restoration with the GT algorithm. For the SLT algorithm, it is difficult to conclude, the two ROC curves being too close. The Dice curve achieves a maximal value of 75% for the SLT lane-marking extraction algorithm on restored images, compared to a maximal value of 73% on the foggy images. This illustrates the advantage of the restoration for lane-marking extraction. The value of the threshold with maximum dice is 50 which is similar to the optimal value obtained on a larger database without fog, see [13]. The optimal threshold is only 23 without restoration. This means that the visibility restoration produces images with properties similar to images without fog, with respect to a lane-marking extraction task. Therefore, visibility restoration used as a pre-processing step allows to use lane-marking extraction as usual with the same tuning.

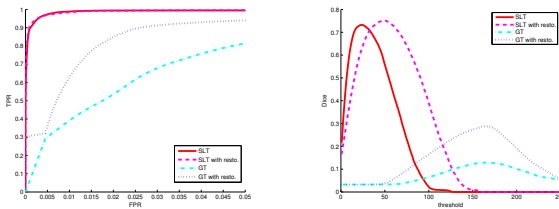


Figure 10. ROC and Dice curves obtained for GT and SLT lane-marking extraction algorithm with and without visibility restoration. A ROC curve displays the True Positive Rate (TPR) versus the False Positive Rate (FPR) for different values of the extraction threshold. The Dice curve displays  $\frac{2TP}{(TP+FP)+P}$  versus the extraction threshold and is dedicated to the detection of small objects.

To illustrate the stability obtained with the proposed tone mapping step along time, a gray level video before and after visibility restoration ( $p = 0.95$ ,  $s_v = 61$  and  $s_i = 5$ ) is supplied as additional material.

## 5. Conclusion

We set the visibility restoration from a single image without using any extra information as a particular filtering problem and we thus proposed a novel algorithm based on median filter. Its main advantage is its speed since its complexity is only a linear function of the input image size and it also achieves as good or even better results compared to state of the art algorithms as illustrated in the experiments. We have also proposed a new filter which preserves edges and corners with obtuse angle as an alternative to the median filter but other operators dedicated to visibility restoration allowing to infer the atmospheric veil can be also imag-

ined. The proposed algorithm, thanks to its speed, may be used with advantages as pre-processing in many systems ranging from surveillance, intelligent vehicles, to remote sensing.

## References

- [1] R. Fattal. Single image dehazing. In *ACM SIGGRAPH'08*, pages 1–9, New York, NY, USA, 2008. ACM.
- [2] N. Hautière, J.-P. Tarel, and D. Aubert. Towards fog-free in-vehicle vision systems through contrast restoration. In *IEEE Conference on Computer Vision and Pattern Recognition (CVPR'07)*, pages 1–8, Minneapolis, Minnesota, USA, 2007.
- [3] N. Hautière, J.-P. Tarel, D. Aubert, and E. Dumont. Blind contrast enhancement assessment by gradient ratioing at visible edgese. *Image Analysis & Stereology Journal*, 27(2):87–95, june 2008.
- [4] N. Hautière, J.-P. Tarel, J. Lavenant, and D. Aubert. Automatic fog detection and estimation of visibility distance through use of an onboard camera. *Machine Vision and Applications*, 17(1):8–20, april 2006.
- [5] K. He, J. Sun, and X. Tang. Single image haze removal using dark channel prior. In *IEEE Conference on Computer Vision and Pattern Recognition (CVPR'09)*, pages 1956–1963, 2009.
- [6] J. Kopf, B. Neubert, B. Chen, M. Cohen, D. Cohen-Or, O. Deussen, M. Uyttendaele, and D. Lischinski. Deep photo: Model-based photograph enhancement and viewing. *ACM Transactions on Graphics (SIGGRAPH Asia'08)*, 27(5):116:1–116:10, 2008.
- [7] S. G. Narashiman and S. K. Nayar. Interactive deweathering of an image using physical model. In *IEEE Workshop on Color and Photometric Methods in Computer Vision*, October 2003.
- [8] S. G. Narasimhan and S. K. Nayar. Contrast restoration of weather degraded images. *IEEE Transactions on Pattern Analysis and Machine Intelligence*, 25(6):713–724, June 2003.
- [9] S. Perreault and P. Hebert. Median filtering in constant time. *IEEE Transactions on Image Processing*, 16(9):2389–2394, september 2007.
- [10] P. Shirley, J. Ferwerda, E. Reinhard, and M. Stark. Photographic tone reproduction for digital images. In *ACM SIGGRAPH'02*, pages 267–276, 2002.
- [11] S. Shwartz, E. Namer, and Y. Schechner. Blind haze separation. In *IEEE Conference on Computer Vision and Pattern Recognition (CVPR'06)*, pages II: 1984–1991, 2006.
- [12] R. Tan. Visibility in bad weather from a single image. In *IEEE Conference on Computer Vision and Pattern Recognition (CVPR'08)*, pages 1–8, 2008.
- [13] T. Veit, J.-P. Tarel, P. Nicolle, and P. Charbonnier. Evaluation of road marking feature extraction. In *Proceedings of 11th IEEE Conference on Intelligent Transportation Systems (ITSC'08)*, pages 174–181, Beijing, China, 2008.